Here, $\bar{x}_{a,hem}$ is the hemispheric mole fraction, x_a^i are the measured atmospheric mole fractions of the compound, n_a and n_{hem} are the total number of moles in the atmosphere and hemisphere, respectively, ($n_a = 1.77 \times 10^{20}$ mol), and Θ_i and Θ_{i-1} are, respectively, the latitudes at the beginning and at the end of each incremental interval. Constant mixing ratios were assumed between 45.3° and the North Pole (11.55 ppt) and between −53.3° and the South Pole (8.25 ppt).

18. If we change the ITCZ from 0° to 5°N, the hemispheric means change from 11.1 to 11.3 ppt for the NH and from 8.5 to 8.6 ppt for the SH.
19. The saturation anomaly (in percent) is defined as the departure of the observed dissolved amount from equilibrium:

$$\Delta_g = 100\left(\frac{p_w - p_a}{p_a}\right) \quad (3)$$

where p_w and p_a are the partial pressures of the gas in water and air, respectively. Because inert compounds like CFC-11 do not react with seawater, the departures of their surface partial pressures from equilibrium are directly attributable to physical processes, such as warming and cooling, advection, or mixing, and can be used under certain conditions to factor out physical effects for gases that are not conservative in the surface ocean (*15*). In Eq. 1, a net saturation anomaly is calculated by subtracting the CFC-11 saturation anomaly from the observed anomaly of CH_3Br.
20. H. J. McLellan, *Elements of Physical Oceanography* (Pergamon, Oxford, 1965). Nitrous oxide is a strong indicator for upwelling regions and was measured during this cruise in both air and surface water with a GC-ECD system.
21. J. H. Ryther [*Science* **166**, 72 (1969)] assumed 9.9% for coastal waters including offshore areas of high productivity and 0.1% for regions of intense upwelling. H. W. Menard and S. M. Smith [*J. Geophys. Res.* **71**, 4305 (1966)] showed that 7.5% of the ocean is shallower than 200 m, the classical definition of coastal waters. Because we found positive CH_3Br saturation anomalies in waters deeper than 200 m and have included less intense areas of upwelling in our estimate, we assigned 10% of the ocean to each of these regions.
22. S. Elliot and F. S. Rowland, *Geophys. Res. Lett.* **20**, 1043 (1993); W. Mabey and T. Mill, *J. Phys. Chem. Ref. Data* **7**, 383 (1978).
23. One residual standard deviation from a fit of atmospheric data to a locally weighted, statistical smoothing (LOESS) algorithm was 0.6 ppt [W. S. Cleveland, *J. Am. Stat. Assoc.* **74**, 829 (1979)].
24. E. Kossina, *Inst. Meereskunde Veröff. Geogr.-Naturwiss.* **9**, 70 (1921).
25. The partial atmospheric lifetime τ_0, with respect to oceanic loss is computed from

$$\frac{1}{\tau_0} = \frac{AK_w}{HM}\left(\frac{zk_s + \sqrt{k_zD_z}}{zk_s + K_w + \sqrt{k_zD_z}}\right) y^{-1} \quad (4)$$

with the area of the ocean $A = 361 \times 10^{12}$ m^2, the mean depth of the mixed surface water layer $z = 75$ m [see Y.-H. Li, T.-H. Peng, W. S. Broecker, H. G. Östlund, *Tellus B* **36**, 212 (1984)], the reciprocal solubility H for each oceanic regime (Table 2), the mass of the atmosphere $M = 1.77 \times 10^{20}$ mol, the air-sea exchange coefficient K_w (Table 2), and the in situ degradation rate k_s (*1*). The term for downward transport $\sqrt{k_zD_z}$ is calculated from an in-situ degradation rate k_z at an estimated thermocline temperture and the diffusivity D_z given by Li *et al.*
26. *Global Ozone Research and Monitoring Project (WMO Rep. 25*, World Meteorological Organization, Geneva, 1991). Mellouki *et al.* (*12*) included stratospheric losses in their estimate, whereas Zhang *et al.* (*13*) did not. We used a stratospheric lifetime of 50 years from the WMO report to adjust the number of Zhang *et al.*
27. J. M. Lobert *et al.*, unpublished results from *Polarstein* cruise ANT XII-1, October to November 1994.
28. R. Wanninkhof, *J. Geophys. Res.* **97C**, 7373 (1992).
29. This study was funded by the Methyl Bromide Global Coalition and the Atmospheric Chemistry Project of NOAA's Climate and Global Change Research Program. We thank M. R. Nowick for electrical expertise, E. Saltzman for critical review, the NOAA–Pacific Marine Environmental Laboratory group for their support, and the helpful crew of the *NOAA Ship Discoverer*.

27 July 1994; accepted 27 December 1994

Iceberg Discharges into the North Atlantic on Millennial Time Scales During the Last Glaciation

Gerard C. Bond and Rusty Lotti

High-resolution studies of North Atlantic deep sea cores demonstrate that prominent increases in iceberg calving recurred at intervals of 2000 to 3000 years, much more frequently than the 7000- to 10,000-year pacing of massive ice discharges associated with Heinrich events. The calving cycles correlate with warm-cold oscillations, called Dansgaard-Oeschger events, in Greenland ice cores. Each cycle records synchronous discharges of ice from different sources, and the cycles are decoupled from sea-surface temperatures. These findings point to a mechanism operating within the atmosphere that caused rapid oscillations in air temperatures above Greenland and in calving from more than one ice sheet.

The pioneering studies by Ruddiman and his colleagues of the North Atlantic's glacial record demonstrated that the amounts of drifting glacial ice were closely tied to Milankovitch-forced growth and decay of Northern Hemisphere ice sheets (*1–3*). Subsequent work on North Atlantic sediment from the last glacial cycle revealed in addition a higher frequency of iceberg discharges, about every 7000 to 10,000 years, that have come to be known as Heinrich events (*4, 5*). A leading explanation for the Heinrich events is surging of ice in Hudson Strait (*6*). Glaciological models, however, do not readily explain two recent findings. One is that five of the six Heinrich events occurred at the culminations of progressive coolings and were followed precipitously by warmings to almost interglacial temperatures (*7*). The second is that the youngest Heinrich event was nearly synchronous with rapid disintegration of the Barents ice sheet (*8*). In this paper we report results from high-resolution analyses of deep sea cores that bear further on mechanisms for ice-rafting events in the North Atlantic.

One of these findings is the presence of ice-rafting cycles in the intervals between Heinrich events. We identified these cycles, defined by variations in lithic concentrations [see also (*9*)], in two cores, DSDP site 609 and VM23-81 (Figs. 1 and 2). The records from the two cores match well (Fig. 2). Because the cores are separated by nearly 5° of latitude and are in different depositional environments, the correlation is not an artifact of local ocean surface or sea floor processes. Including the Heinrich events, there are 13 ice-rafting cycles in the interval from 10,000 to 38,000 radiocarbon years ago, yielding an average cycle duration of between 2000 and 3000 years (Fig. 2).

The evidence of a 2000- to 3000-year ice-rafting cycle in the North Atlantic is an intriguing result for it recalls the spacing of the Dansgaard-Oeschger temperature cycles (*10*), so convincingly documented by the measurements of $\delta^{18}O$ in ice from the recent drilling at Summit, Greenland (*11*). To investigate this relation further, we compared the $\delta^{18}O$ record in the GRIP ice core with lithic cycles in VM23-81 (Fig. 3). We first pinned the two records at the peak Younger Dryas cooling and then stretched the deep sea record until H4 matched the equivalent level in the ice identified by Bond and others (*7*). Below H4 the deep sea record was clipped and stretched again until the oldest peak in both records matched. Although the correlation was achieved with fewer clippings and stretchings than in (*7*), it is essentially the same. Between the Younger Dryas and H2, GRIP and GISP2 ages (*11, 12*) agree, within error, with ^{14}C to calendar age conversions (*13*). In addition, a sample of *Acropora palmata* from Barbados has a ^{14}C age of ~27,000 years ago and a U/Th age of 30,500 years ago (*13*), corroborating the GISP2 chronology we infer for the marine record (Fig. 3).

Our correlation demonstrates that all but one Dansgaard-Oeschger cycle corresponds to a lithic peak in the marine record (Fig. 3), indicating a close link between the shifts in air temperatures above Greenland and the ice-rafting cycles. Lithic peaks a, b, and c (Fig. 3), however, occur within the puzzling interval that lacks Dansgaard-

Lamont-Doherty Earth Observatory of Columbia University, Palisades, NY 10964, USA.

Oeschger cycles. Apparently, in that interval the forcing mechanism was more strongly imprinted in the ice-rafting signal than in Greenland ice.

Because most of the lithic cycles between the Heinrich events occur at times of lowered air and sea surface temperatures, it is possible that they simply reflect the increased survivability of icebergs as ocean surface temperatures dropped [for example, (*3*, *5*)]. If that were the case, the pacings and amplitudes of the lithic cycles and of ocean surface temperatures should be similar. The structure of the two records, however, is clearly discordant. For example, the ice-rafting record lacks the distinct longer-term rampings in sea surface coolings, such as began about 33,000 and 38,000 ^{14}C years ago (Fig. 3). Lithic cycles f, g, and h and the two below H4 clearly lag the increase in sea surface coolings as well (Fig. 3). Furthermore, just below and within H3, lithic concentrations are relatively low even though the interval is saturated with the polar foraminifera *Neogloboquadrina pachyderma* (left coiling). In contrast, in other intervals saturated with that foraminifera, lithic concentrations drop abruptly to near-ambient levels, such as in the interval containing cycles a to c, between cycles H2 and d, and between cycles H3 and f (Fig. 3). Because changes in ocean surface circulation would likely be accompanied by changes in surface temperatures, we rule out any mechanism requiring significant changes in iceberg trajectories. We conclude, therefore, that the amount of glacial ice discharged into the North Atlantic Ocean increased suddenly every 2000 to 3000 years.

To investigate further the origin of the lithic cycles, we measured the abundances of 15 lithic grain types (*14*) in DSDP 609 and VM23-81 at a resolution of between 300 and 500 years. We found distinct peaks in three types; fresh, basaltic glass derived from Iceland (*15*), grains with hematite coatings (mostly quartz and feldspar) derived from any of the extensive red bed deposits in the region (Fig. 1), and detrital carbonate grains that came mainly from carbonate rocks in eastern and northern Canada (*5*, *16*) (Fig. 1). The peaks rise above an ambient background composed mostly of quartz and feldspar and less than about 10% of grains with hematite coatings.

In addition to the peaks in detrital carbonate at the levels of the Younger Dryas and H1, H2, and H4 already documented (*5*), we found a narrow peak of carbonate grains at the level of H3 (Fig. 4). This is in contrast to the results of earlier work at lower resolution, which suggested that H3 lacked detrital carbonate grains in the eastern North Atlantic (*5*). Compositions of lithic grains in a high sedimentation rate core, EW9303-31, on the turbidite-free crest of Orphan Knoll in the southwestern Labrador Sea (Fig. 1) are further evidence that detrital carbonate–bearing ice exited the Labrador Sea during the Younger Dryas and during Heinrich events 1, 2, 3, and 4 (Fig. 5) [see also (*17*)]. Isotopic results of Grousset *et al.* (*18*) pointed to sources in Europe for sediment in H3, but their bulk analyses may reflect the compositions of non–ice-rafted fine-grained material. Heinrich event 3 differs from the other Heinrich events, however, in that it has an unusually low concentration of lithic grains.

The other two grain types, basaltic glass and hematite-coated clasts, form a series of prominent compositional cycles that correspond directly to all but one of the lithic peaks (Fig. 4). The increases in ice-rafted debris from specific sources are further evidence against ocean surface coolings as the sole cause of the lithic cycles. More importantly, the evidence points to nearly synchronous changes in the rates of iceberg discharges from the sources of the basaltic glass and hematite-coated grains. In Heinrich events 1, 2, and 4, the abundances of basaltic glass and hematite-coated grains first increase, then drop sharply to low values at the levels where detrital carbonate grains begin to increase (Fig. 4). The picture that emerges is of recurring increases in the discharges of icebergs from the sources of basaltic glass and hematite-coated grains; at the time of Heinrich events 1, 2, and 4, sediment deposited from those icebergs apparently was diluted to trace amounts by the huge additions of sediment from ice exiting the Labrador Sea.

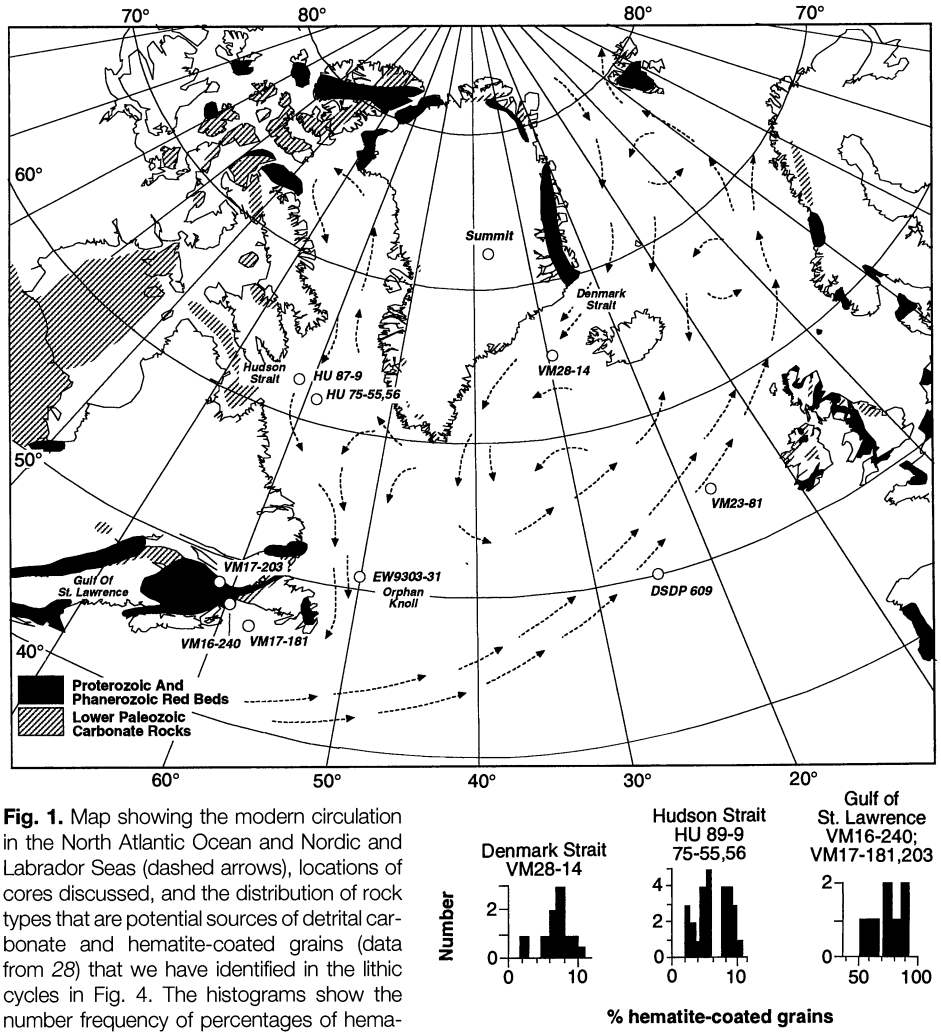

Fig. 1. Map showing the modern circulation in the North Atlantic Ocean and Nordic and Labrador Seas (dashed arrows), locations of cores discussed, and the distribution of rock types that are potential sources of detrital carbonate and hematite-coated grains (data from *28*) that we have identified in the lithic cycles in Fig. 4. The histograms show the number frequency of percentages of hematite-coated grains from 63 to 150 mm across in samples from the indicated cores. For VM28-14, grains were counted in samples containing each of the peaks in basaltic glass (Fig. 5). For the cores near Hudson Strait, grains were counted in samples every 10 cm beginning 60 cm above H1, then from between H1 and H2, and from between H2 and H4(?). In cores from the Gulf of St. Lawrence, grains were counted in samples from within and between the "brick red layers" (*29*); the uppermost of those layers has an AMS radiocarbon age of 13,300 years (*24*). The sampled interval probably extends to close to Termination 1. As explained in the text, we measured the abundances of hematite-coated grains in these places as an aid in identifying possible sources of those grains in ice-rafted sediment in the eastern North Atlantic.

The Icelandic source of the basaltic glass is confirmed by the presence of correlatives of the peaks in dark glass in a core much closer to Iceland, VM28-14, and by evidence that peak abundances of basaltic glass in that core are much larger than in the eastern North Atlantic (Fig. 5). In addition, microprobe analyses on basaltic glass from VM28-14 indicate compositions at the levels of the Younger Dryas, H1, 16,500 years ago, H2, and H3 that are consistent with the geochemistry of rocks in the rift zone in Iceland, perhaps mainly in the northern part of the island (*20*). Although it is possible that the dark glass at the level of the

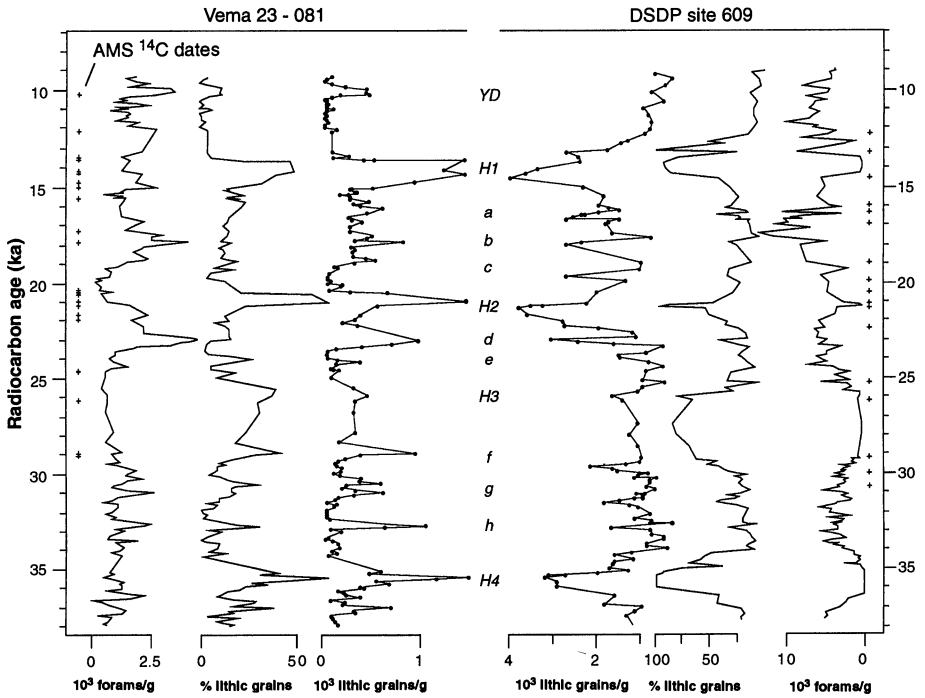

Fig. 2. Lithic and foraminiferal concentrations, in numbers of grains >150 μm per gram of sediment, and the percentage of lithic grains measured relative to the sum of lithic grains and foraminifera >150 μm in sediment from DSDP 609 and VM23-81 (Fig. 1). The records from the two cores face in to emphasize the correlation. Radiocarbon ages given by a (+) and the age models are from (*5, 7*). Both cores reveal prominent cycles in lithic concentrations at the levels of Heinrich layers and in-between these levels as well. The concentrations of foraminifera and the percentages of ice-rafted debris were originally part of the definition of Heinrich events in (*4, 5, 30*). Low foram zones, which are so prominent in DSDP 609, are less dramatic in VM23-81 however, and are absent at the level of Heinrich event 4. The percentages of lithic grains delimits the Heinrich events as they were originally defined (*30*), through either a decrease in foraminiferal concentration, an increase in lithic concentration, or a combination of both. The record of lithic percentages does not, however, delimit all of the ice-rafting cycles. Hence, lithic concentrations are the best indicator of ice-rafting events.

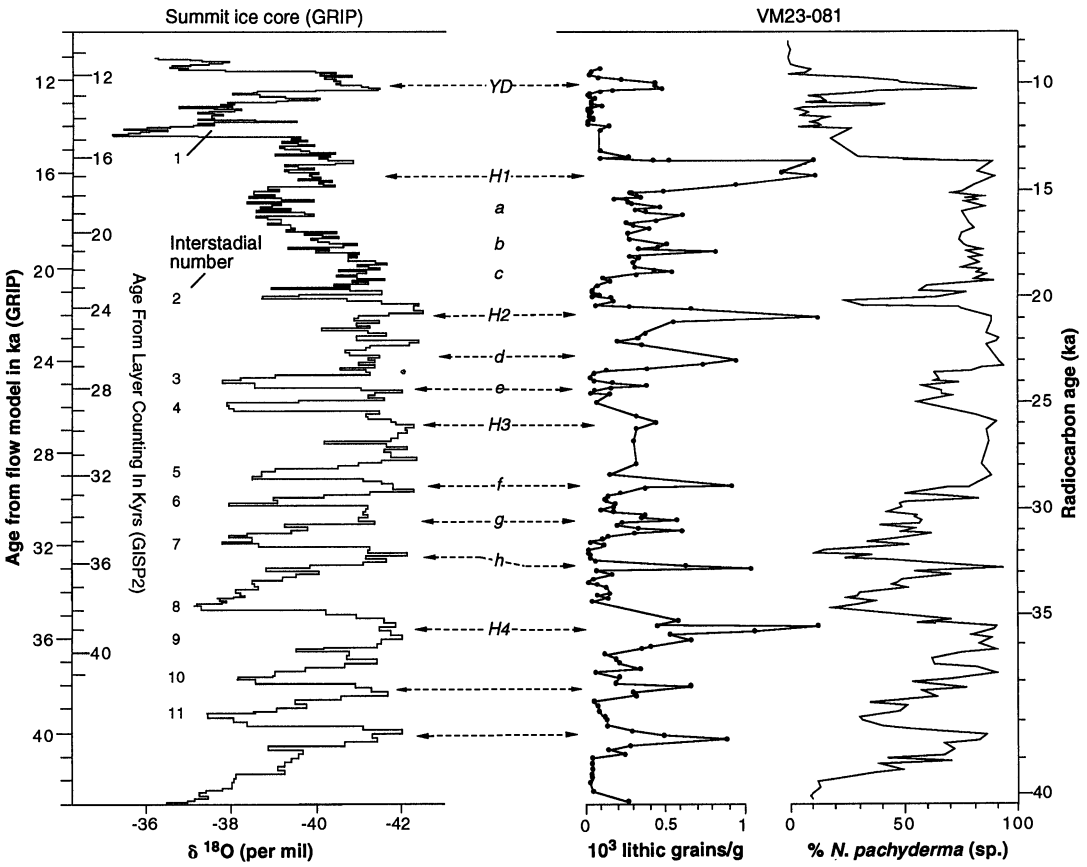

Fig. 3. Comparison of the oxygen isotope record and age model for the GRIP ice core, Summit, Greenland (*11*), with measurements of lithic concentrations (as in Fig. 2) and percentages of the planktic foraminifera *Neogloboquadrina pachyderma* (left coiling), a proxy for surface water temperatures, in VM23-81 (*7*). That foraminifera today lives in waters <10°C and comprises about 95% of the fauna at summer temperatures of <5°C. Age model for the marine record is the same as in Fig. 2. Coring sites are located in Fig. 1. Cycles between the Heinrich events are given letters to aid their description in the text. We find a striking match between the lithic concentration cycles and the temperature cycles in the ice core; the match of the lithic cycles to the ocean surface temperatures, however, is much poorer. We included the GISP2 time scale derived from layer counting to 41,000 years for comparison with the GRIP time scale and the ^{14}C time scale. The GISP2 time scale was transferred into the GRIP record at the sharp interstadial boundaries, which are precisely located in both ice core records (*11, 12*), and then the ages were interpolated between those boundaries. The progressive difference in ages, reaching about 10% at 40,000 calendar years ago, is consistent with error estimated for the ice core dating (*31*).

Younger Dryas came from glacial icebergs and sea ice covered with debris from the eruption which produced the Vedde Ash (*15*), a similar origin is hardly likely for every one of the earlier cycles (*21*). Also, the sulfate record from the GISP2 core reveals no evidence of ash falls at the time of each Dansgaard-Oeschger cycle (*12*).

To narrow the sources of hematite-coated grains we measured the abundances of those grains in cores that lie along the likely major iceberg trajectories into the North Atlantic during the last glaciation. One of these cores is VM28-14 in the southern Denmark Strait (Fig. 1). This coring site monitors the passage of icebergs from East Greenland, Svalbard, around the Arctic Ocean, and western Europe, as suggested by

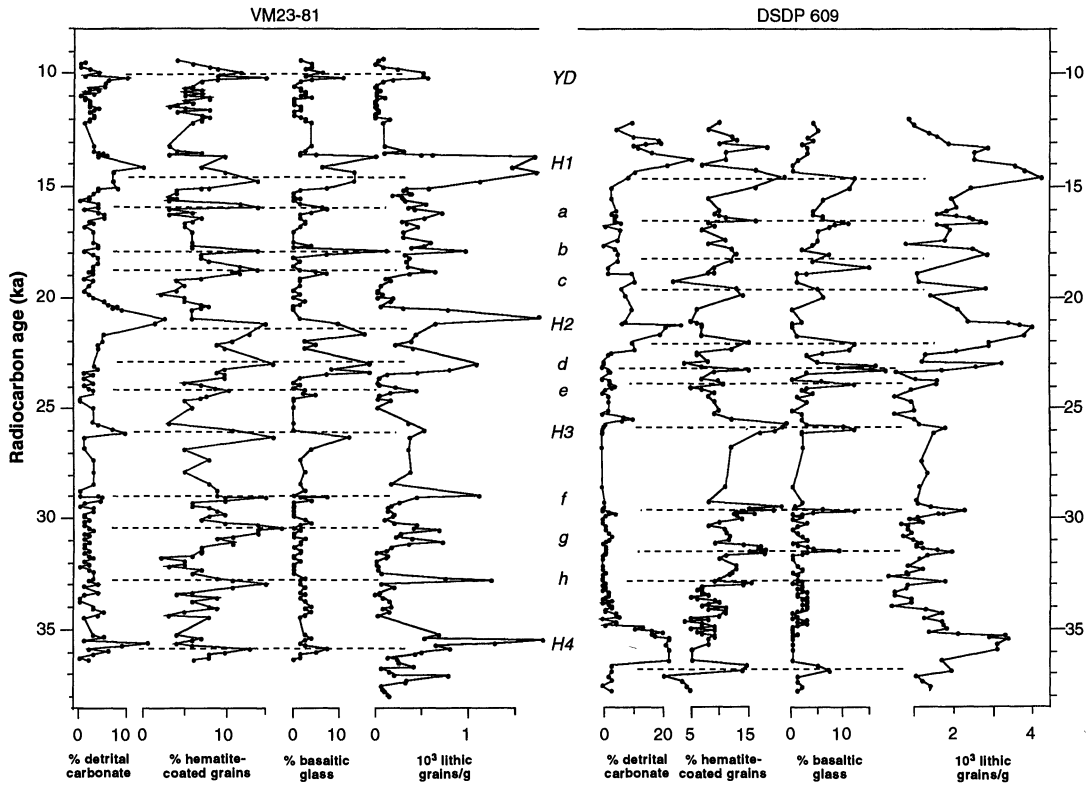

Fig. 4. Measurements of the abundances of three grain types, detrital carbonate, basaltic glass, and hematite-coated grains, in sediments from DSDP 609 and VM23-81 (located in Fig. 1). Age models are from Fig. 2. Lithic cycles labeled as in Fig. 2. Peak abundances in both basaltic glass and hematite-coated grains occur at the peak concentrations of lithic grains in each lithic cycle in both cores. At the Heinrich events and the Younger Dryas, peak abundances in a third grain type, detrital carbonate, are present as well. We found a narrow peak in detrital carbonate at the level of H3 in both cores, which did not appear in much coarser analyses done previously (*5*). To measure these grain types we first embedded a small amount of the 63- to 150-μm fraction from each sample in glycerin on a glass slide. Using a petrographic microscope we line-counted 200 lithic grains to obtain a measure of the percentage of each tracer by number. We chose a relatively small grain size for greater accuracy in petrographic identification; we found that no compositional bias was introduced from counting smaller grains, however, by comparing the results with grain counts in the >150-μm fraction across compositional cycles in VM23-81.

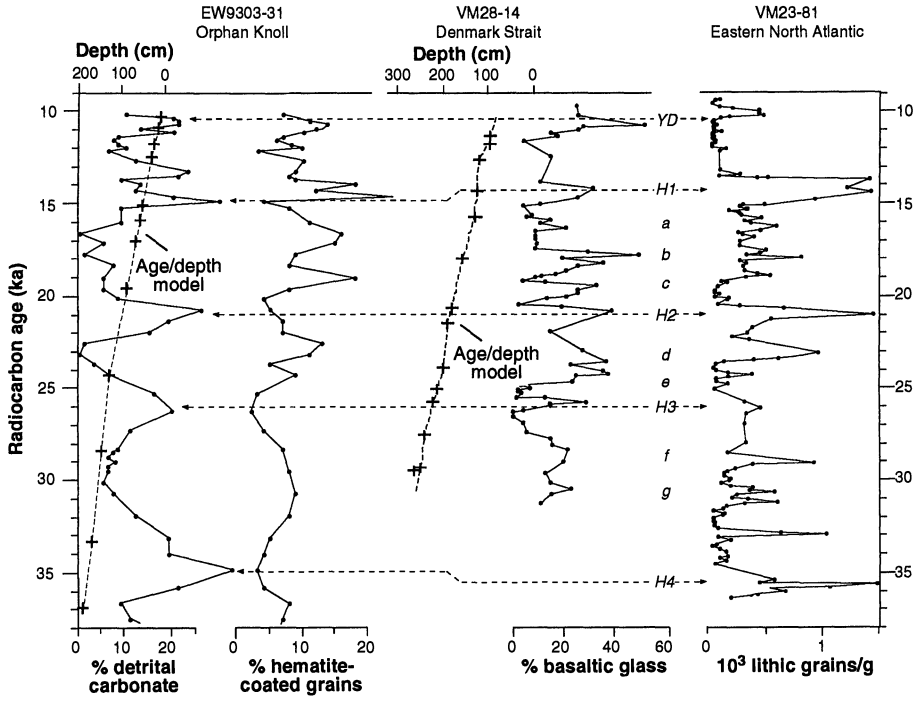

Fig. 5. Lithic cycles in VM23-81 (from Fig. 2) compared with abundances of grain types measured in a core from the southern part of Denmark Strait and from Orphan Knoll, an elevated block of crust in the southwestern Labrador Sea (Fig. 1). Accelerator radiocarbon ages in Orphan Knoll from Zurich; in VM28-14 the upper four accelerator dates are from S. Lehman (*32*) and the rest are accelerator dates from Zurich. A reservoir correction of 400 years has been subtracted from the ^{14}C measurements. Peak abundances in basaltic glass in VM28-14 match each lithic peak in VM23-81, demonstrating a remarkable degree of coherency between the two records. In the Orphan Knoll core, our measurements of detrital carbonate confirm the presence of a source of detrital carbonate–bearing icebergs in the Labrador Sea, including that for H3.

the present-day circulation (Fig. 1) and reconstructions of the full glacial circulation (*1–3, 22*). Cores HU89-9 and HU75-55, in the western Labrador Sea off Hudson Strait, lie beneath a second major pathway, that of Laurentide ice exiting Hudson Strait together with any ice from northern Canada and Greenland (Fig. 1). Finally, sites VM17-181, VM17-203, and VM16-240, in and just offshore of the Gulf of St. Lawrence (Fig. 1), monitor the passage of icebergs calved from another large outlet of Laurentide ice (*23*).

The maximum abundances of hematite-coated grains are about 10% in the southern Denmark Strait and in the Labrador Sea (Fig. 1), but they are much greater, up to 95%, in and near the Gulf of St. Lawrence. Hence, because the percentages of hematite-coated grains in each lithic peak in VM23-81 and DSDP site 609 are well above 10% (Fig. 4), discharge of ice from the Gulf of St. Lawrence must have increased during each lithic cycle (*24*). Similarly, in the core from Orphan Knoll, hematite-coated grains exceed 10% at levels correlative with some, but not all of the cycles in the eastern North Atlantic (Fig. 5). Ice from the Gulf of St. Lawrence perhaps did not drift to Orphan Knoll, and red beds in Newfoundland could have supplied the required number of hematite-coated grains (Fig. 1).

Our compositional data do not rule out iceberg discharges from the Greenland, Barents, and Scandinavian ice sheets. We have limited our analyses to a few key and easily recognizable grain types. In addition, sediment-laden icebergs from more northerly sources may not have reached the eastern North Atlantic.

The results of this study suggest that every 2000 to 3000 years, coincident with the Dansgaard-Oeschger coolings, ice within the Icelandic ice cap and probably within or near the Gulf of St. Lawrence underwent nearly synchronous increases in rates of calving. Hence, it is improbable that the calving cycles were forced by an internal process analogous to the surging of a glacier. Instead, the cycles must reflect the operation of climate upon unstable ice, probably within ice streams or ice shelves. Those cycles in which the Dansgaard-Oeschger coolings lead the increases in ice-rafted debris (Fig. 3) suggest that iceberg discharges occurred when air temperatures dropped across a critical threshold.

Although the Heinrich events were originally thought to be the dominant features of the North Atlantic's deep sea record, our findings demonstrate that they are superimposed on the rhythm of the climate-forced ice-rafting events. The Heinrich events reflect another, slower rhythm tied to the massive discharges in Hudson Strait. An unexpected result of our compositional measurements is the evidence that the two rhythms may be linked. Each discharge of detrital carbonate–bearing ice from Hudson Strait lags just slightly the discharge from the other two sources (Fig. 4). Perhaps sudden Dansgaard-Oeschger coolings triggered the discharges in Hudson Strait at nearly the same time as discharges from the other sources. Alternatively, the trigger could have been the rise of sea level that must accompany each 2000- to 3000-year flood of icebergs into the ocean (*25*). The sea level mechanism is consistent with the slight lag in the discharges from Hudson Strait. Moreover, the amount of ice entering the ocean each time might have been quite large if other ice sheets farther north discharged icebergs at the same time. In either case, a binge-purge model can explain the slower pacing of Heinrich events as a consequence of the time it took for Hudson Strait ice to recover from a massive discharge and reach an unstable condition in which another discharge might be triggered (*6*).

Our findings also bear on the question of what caused the sudden changes in glacial climates revealed by the Dansgaard-Oeschger cycles. Ocean circulation models suggest that injections of fresh water into the North Atlantic can alter the ocean's heat conveyor and cause abrupt shifts in North Atlantic sea surface and air temperatures (*26*). A possible source of fresh water is the discharge of icebergs from surging ice sheets. Yet the iceberg discharges we have identified, including those from Hudson Strait, appear to have been triggered by climate or a climate-related mechanism rather than vice versa. Perhaps a recurring internal process in another ice sheet discharged enough ice each time to alter the North Atlantic's heat conveyor, and the resulting ocean surface coolings triggered the iceberg discharges we have identified. If so, a large ice sheet, perhaps in Greenland, in the Barents Sea, or in Scandinavia, must have collapsed every 2000 to 3000 years. It is also possible, though, that the Dansgaard-Oeschger coolings reflect a recurring climate-driven mechanism that triggered discharges from ice sheets, and the impact of meltwater on the heat conveyor only amplified the temperature shifts. In this regard it is interesting that climate shifts with pacings not unlike those we have identified for the ice rafting events appear to be present in a number of Holocene climate records, including advances of mountain glaciers in both hemispheres (*27*).

REFERENCES AND NOTES

1. W. F. Ruddiman, *Geol. Soc. Am. Bull.* **88**, 1813 (1977).
2. W. F. Ruddiman and A. McIntyre, *Palaeogeogr. Palaeoclimatol. Palaeoecol.* **35**, 145 (1981).
3. F. W. Smythe Jr., W. F. Ruddiman, D. N. Lumsden, *Mar. Geol.* **64**, 131 (1985).
4. W. S. Broecker *et al.*, *Clim. Dyn.* **6**, 265 (1990).
5. G. Bond *et al.*, *Nature* **360**, 245 (1992).
6. D. R. MacAyeal, *Paleoceanography* **8**, 767 (1993); *ibid.*, p. 775; R. B. Alley and D. R. MacAyeal, *ibid.* **9**, 503 (1994).
7. G. Bond *et al.*, *Nature* **365**, 14 (1993).
8. J. F. Bischof, *Mar. Geol.* **117**, 35 (1994).
9. Lithic concentration is defined as numbers of lithic grains > 150 μm per gram of sample. Our measurements of lithic concentrations from DSDP 609 differ from earlier ones made in the same core (*4*). For the earlier measurements, samples were washed to preserve all foraminifera; this unavoidably left much of the fine lithic fraction in aggregates coarser than 150 μm. Our revisions to the lithic data were made by rewashing and recounting samples containing fine-fraction aggregates. The correlation of the DSDP 609 lithic record with that from VM23-81, in which aggregates of fine fraction are rare, attests to the validity of the lithic records in both cores.
10. W. Dansgaard, H. G. Clausen, N. Gunderstrup, S. J. Johnsen, G. Rygner, in *Greenland Ice Core: Geophysics, Geochemistry, and the Environment*, C. C. Langway, H. Oeschger, W. Dansgaard, Eds. (*Geophys. Monogr. 33*, American Geophysical Union, Washington, DC, 1985), pp. 71–76.
11. W. Dansgaard *et al.*, *Nature* **364**, 218 (1993).
12. P. A. Mayewski *et al.*, *Science* **263**, 1747 (1994).
13. E. Bard *et al.*, *Radiocarbon* **3**, 191 (1993).
14. The grain types counted are: quartz, feldspar, volcanic rock fragments (acidic and basaltic where the distinction could be made), metamorphic rock fragments, carbonate rock fragments, siliclastic rock fragments, chert, glauconite, mafic grains (hornblende, pyroxene, and olivene), dark basaltic glass and palagonite, clear rhyolitic glass, and hematite-coated grains. Hematite-coated grains are defined as grains with 5% or more hematite staining. The abundances of hematite-stained grains do not include counts of rhyolitic and basaltic glass and reddish basalt clasts which could come from oxidized flow tops.
15. M. N. Bramlette and W. H. Bradley, *U.S. Geol. Surv. Prof. Pap. 196-A*, 1 (1941); G. P. L. Walker *et al.*, *Site 115, Init. Rep. Deep Sea Drill. Proj. Red* **12**, 361 (1972); W. F. Ruddiman and L. K. Glover, *Geol. Soc. Am. Bull.* **83**, 2817 (1972); J. Sjøholm *et al.*, *J. Quat. Sci.* **6**, 159 (1991).
16. J. T. Andrews and K. Tedesco, *Geology* **20**, 1087 (1992); J. T. Andrews, H. Erlenkeuser, K. Tedesco, A. Aksu, A. J. T. Jull, *Quat. Res.* **41**, 2 (1994).
17. The peak in grains of detrital carbonate we have identified at the level of H3 cannot be as old as the event at ~29,000 years assigned tentatively to H3 in a core from the flank of Orphan Knoll (*19*).
18. F. E. Grousset *et al.*, *Paleoceanography* **8**, 175 (1993).
19. C. Hillaire-Marcel, A. DeVernal, G. Bilodeau, G. Wu, *Can. J. Earth Sci.* **31**, 63 (1994).
20. K. Gronvold, personal communication.
21. Moreover, eruptions correlating so precisely with the Dansgaard-Oeschger cycles are extremely unlikely.
22. Although ice may have drifted east as well as west of Iceland, Ruddiman (*1*) regarded the enormous amounts of ice-rafted debris in the vicinity of VM28-14 as evidence that ice along both routes converged in the southern part of the Denmark Strait. Ruddiman (*1*) also discounted the importance of ice flowing directly southward from Scandinavia into the subpolar North Atlantic owing to the strength of the West Wind Drift.
23. G. H. Denton and T. J. Hughes, in *The Last Great Ice Sheets* (Wiley, New York, 1981).
24. We have an AMS radiocarbon age (from the University of Arizona lab) for the top of the uppermost "brick red till" in VM 17-203 (*29*) (Fig. 1) of 13,300 years (with a 400-year reservoir correction subtracted from the ^{14}C measurement), suggesting that this layer is correlative with the peak in abundance of hematite-coated grains at ~13,500 years in DSDP site 609 (Fig. 4).
25. G. C. Bond and R. Lotti, *Eos (Fall Suppl.)* **75**, 54 (1994).

26. W. Broecker *et al.*, *Clim. Dyn.* **6**, 265 (1992); W. S. Broecker, *Nature* **372**, 421 (1994); L. D. Keigwin and S. J. Lehman, *Paleoceanogr. Currents* **9**, 185 (1994); D. Paillard and L. Labeyrie, *Nature* **372**, 162 (1994); S. Rahmstorf, *ibid.*, p. 82.
27. G. H. Denton and W. Karlen, *Quat. Res.* **3**, 155 (1973); W. Dansgaard *et al.*, in *Climate Processes and Climate Sensitivity*, J. E. Hansen and T. Takahashi, Eds. (*Geophys. Monogr. 29*, American Geophysical Union, Washington, DC, 1984), pp. 288–298; F. Rothlisberger *et al.*, *Verlag Sauerlander* (AT Verlag, Aarau, Switzerland, 1986); M. Magny, *Quat. Res.* **40**, 1 (1993).
28. J. K. A. Habicht, in *Paleoclimate, Paleomagnetism, and Continental Drift*, M. K. Horn, Ed. (American Association of Petroleum Geologists, Tulsa, OK, 1979); R. H. Dott Jr. and R. L. Batten, *Evolution of the Earth* (McGraw-Hill, New York, 1981).
29. J. R. Conolly and M. Ewing, *Nature* **208**, 135 (1965); F. T. Barranco Jr., W. L. Balsam, B. C. Deaton, *Mar. Geol.* **89**, 299 (1989).
30. H. Heinrich, *Quat. Res.* **29**, 142 (1988).
31. R. B. Alley *et al.*, *Nature* **362**, 527 (1993).
32. S. Lehman, personal communication.
33. We thank G. Denton, D. MacAyeal, R. Alley, and T. Sowers for comments on the manuscript, and we acknowledge the able assistance of J. Zweibel, W. Tayler, and T. McMichaels in our analyses. We also thank Tappan Zee High School students V. Tong and W. Wang who volunteered their time to help prepare samples. J. Andrews and M. Kirby kindly gave us samples from cores near Hudson Strait. This project was funded in part by grants from the National Science Foundation and from the National Oceanic and Atmospheric Administration. Samples were provided by Lamont-Doherty Earth Observatory (L-DEO) Deep-Sea Sample Repository which is supported by the NSF and the ONR, and through the assistance of the Ocean Drilling Program. This is L-DEO contribution #5309.

17 October 1994; accepted 28 December 1994

Resonant Tunneling in the Quantum Hall Regime: Measurement of Fractional Charge

V. J. Goldman* and B. Su

In experiments on resonant tunneling through a "quantum antidot" (a potential hill) in the quantum Hall (QH) regime, periodic conductance peaks were observed as a function of both magnetic field and back gate voltage. A combination of the two periods constitutes a measurement of the charge of the tunneling particles and implies that charge deficiency on the antidot is quantized in units of the charge of quasi-particles of the surrounding QH condensate. The experimentally determined value of the electron charge e is 1.57×10^{-19} coulomb = $(0.98 \pm 0.03)e$ for the states $\nu = 1$ and $\nu = 2$ of the integer QH effect, and the quasi-particle charge is 5.20×10^{-20} coulomb = $(0.325 \pm 0.01)e$ for the state $\nu = 1/3$ of the fractional QH effect.

Laughlin (*1*) has explained the exactness of the Hall conductance quantization in the integer quantum Hall effect (QHE) (*2*) as a consequence of a combination of the gauge invariance of the electromagnetic field and the quantization of the charge of the current carriers, the electrons. He considered a gedanken experiment in which a two-dimensional electron system (2DES) forms a finite length cylinder with magnetic field B normal to the surface of the cylinder and additional magnetic flux Φ threaded through the cylinder parallel to its axis. Laughlin showed that if (i) disorder is sufficiently small so that it does not destroy the Landau quantization of the electronic states, (ii) the chemical potential μ lies in the mobility gap between two Landau levels, and (iii) temperature T is small as compared to cyclotron energy, then adiabatic change of Φ by ϕ_0, the flux quantum, is strictly equivalent to the transfer of one electron per Landau level from one edge of the cylinder to the other. This implies that the Hall conductance of such a 2DES sample is quantized exactly to ie^2/h, where i is the number of Landau levels below μ and h is Planck's constant. This gedanken experiment was adapted to Corbino geometry and elaborated by Halperin (*3*).

In a seminal work (*4*), Laughlin related the fractional QHE (*5*) at Landau level filling $\nu = 1/(2k + 1)$ (k is an integer) to the fractional quantization of the charge of elementary charged excitations (quasi-particles) of that state in units of $e^* = e/(2k + 1)$. Halperin (*6*) recognized that Laughlin's quasi-particles could be described by fractional statistics, and Kivelson and Rocek (*7*) have shown that fractionally charged quasi-particles must obey fractional statistics.

It has been argued (*8*) that fractional quantization of Hall conductance implies that the quasi-particles have a charge that is a rational fraction of the electron charge. However, it was subsequently recognized that quantization of Hall conductance is a property of the condensate; for example, the fractional QHE states can be understood within the composite fermion theory (*9*), without explicit consideration of quasi-particles at all. Several experiments have been attempted to determine the charge of quasi-particles (*10*). However, either their interpretations were ambiguous or the measurement can be related to the quantization of Hall conductance. Several theoretical works (*11*, *12*) have considered resonant tunneling (RT) in the QHE regime, which is, in some sense, a microscopic implementation of Laughlin's gedanken experiment. Experimental work was reported on RT in confined quantum dots (*13*) and antidots (*14*), all in the integer QHE and without back gates. However, we are not aware of experimental or theoretical works explicitly predicting quantization of charge deficiency on an antidot.

Here we report experiments on RT through states magnetically bound on a lithographically defined potential hill ("quantum antidot") in the integer and fractional QHE regimes. We see quasi-periodic RT conductance peaks as a function of both the magnetic field B and back gate voltage V_{BG}. We find that a combination of these two measurements for a given ν QHE state constitutes a direct measurement of the charge of the tunneling particles. Our results imply that the charge deficiency on the antidot is quantized in units of the charge of the quasi-particles of the surrounding QHE condensate q. Using this technique, we have measured the electron charge as $q = 1.57 \times 10^{-19}$ C = $(0.98 \pm 0.03)e$ at $\nu = 1$ and $\nu = 2$ and the quasi-particle charge as $q = 5.20 \times 10^{-20}$ C = $(0.325 \pm 0.01)e$ at $\nu = 1/3$.

Samples were fabricated from very low disorder GaAs heterostructure material described in (*15*). The antidot-in-a-constriction geometry was defined by standard electron-beam lithography on a pre-etched mesa with ohmic contacts (Fig. 1). The sample was then chemically etched, and Ag front gates were deposited in the etched trenches; samples were mounted on sapphire substrates with In, which serves as the back gate. The two front gates were contacted independently and were used to vary ν between the gates (in a given B) and to balance the two barriers in the RT regime. We prepared the 2DES with a density $n \approx 1 \times 10^{11}$ cm^{-2} and $\mu \approx 2 \times 10^6$ cm^2 V^{-1} s^{-1} by exposing the sample to red light. Experiments were performed in a dilution refrigerator with sample probe wires filtered at millikelvin temperatures, so that the total electromagnetic background at the sample's contacts is believed to be <2 μV (root mean square). The four-terminal magnetoresistance of the samples $R_{(2\text{-}3;1\text{-}4)}$ (see Fig. 1) was measured with a lock-in amplifier with an excitation of ~ 2 μV.

The etched front gates and antidot cre-

Department of Physics, State University of New York, Stony Brook, NY 11794, USA.

*To whom correspondence should be addressed.